New Member of the "112" Family, $LaBaCo_2O_{5.5}$: Synthesis, Structure, and Magnetism

E.-L. Rautama,[†,‡] V. Caignaert,*[,†] Ph. Boullay,[†] Asish K. Kundu, V. Pralong,[†] M. Karppinen,[‡] C. Ritter,[§] and B. Raveau[†]

Laboratoire CRISMAT, ENSICAEN/CNRS, 6 Bd. du Maréchal Juin, 14050 Caen Cedex 4, France, Laboratory of Inorganic Chemistry, Department of Chemistry, Helsinki University of Technology, P.O. Box 6100, FI-02015 TKK, Finland, and Institut Laue-Langevin, BP 156, 38042 Grenoble Cedex, France

Received August 10, 2008. Revised Manuscript Received October 3, 2008

The outermost member of the 112 family $LaBaCo_2O_{5.5}$ has been synthesized using a multistep method to stabilize its structure. Its structural study, combining neutron powder diffraction and electron microscopy, shows that its orthorhombic matrix consists of layers of corner-shared CoO_6 octahedra interconnected through CoO_5 pyramids like in the other 112 cobaltates but contains small $LaBaMn_2O_{5.5}$-type domains (8%) due to local oxygen displacement. Its magnetic properties and magnetic structure evidence the following features: G-type antiferromagnetic/G-type ferrimagnetic/paramagnetic with $T_N = 260$ K and $T_C = 326$ K. This cobaltate differs from other 112 cobaltates by its antiferromagnetic structure which keeps the same symmetry as its ferrimagnetic phase, probably due to the size effect of La^{3+} upon crystal field. Trivalent cobalt is shown to keep the intermediate spin state in the whole temperature range from 10 to 326 K.

Introduction

During the past decade, the oxygen deficient ordered double perovskite cobaltates with the general formula $LnBaCo_2O_{5.5}$ (Ln = lanthanoid or Y) have drawn significant interest due to their fascinating physical properties.[1−18] These 112 cobalt perovskites exhibit several magnetic transitions, paramagnetic (PM)/ferromagnetic (FM)/antiferromagnetic (AFM), in a wide temperature range. Moreover a semimetal/insulator transition is observed above room temperature. An important issue concerns the possible existence of a spin state transition of cobalt which would explain the magnetic and the semimetal−insulator transitions that are observed in these materials. Besides the studies of many authors[1−18] which suggest this important role of spin state transitions in such properties, there are several reports which disagree with the occurrence of spin state transition in these systems across T_{IM}.[19−23]

Several neutron diffraction studies have been conducted to establish the spin state of cobalt and the magnetic structure in $LnBaCo_2O_{5.5}$ compounds with Ln = Pr, Nd, Tb, Ho, and Y.[6,18,24−30] The models proposed for the magnetic structure of these compounds are all different, and there is controversy even between two different studies on the same compound.[6,18]

[†] ENSICAEN/CNRS.
[‡] Helsinki University of Technology.
[§] Institut Laue-Langevin.

(1) Martin, C.; Maignan, A.; Pelloquin, D.; Nguyen, N.; Raveau, B. *Appl. Phys. Lett.* **1997**, *71*, 1421.
(2) Troyanchuk, I. O.; Kasper, N. V.; Khalyavin, D. D.; Szymczak, H.; Szymczak, R.; Baran, M. *Phys. Rev. Lett.* **1998**, *80*, 3380.
(3) Maignan, A.; Martin, C.; Pelloquin, D.; Nguyen, N.; Raveau, B. *J. Solid State Chem.* **1999**, *142*, 247.
(4) Respaud, M.; Frontera, C.; García-Muñoz, J. L.; Aranda, M. A. G.; Raquet, B.; Broto, J. M.; Rakoto, H.; Goiran, M.; Llobet, A.; Rodríguez-Carvajal, J. *Phys. Rev. B* **2001**, *64*, 214401.
(5) Moritomo, Y.; Akimoto, T.; Takeo, M.; Machida, A.; Nishibori, E.; Takata, M.; Sakata, M.; Ohoyama, K.; Nakamura, A. *Phys. Rev. B* **2000**, *61*, R13325.
(6) Soda, M.; Yasui, Y.; Fujita, T.; Miyashita, T.; Sato, M.; Kakurai, K. *J. Phys. Soc. Jpn.* **2003**, *72*, 1729.
(7) Burley, J. C.; Mitchell, J. F.; Short, S.; Miller, D.; Tang, Y. *J. Solid State Chem.* **2003**, *170*, 339.
(8) Taskin, A. A.; Lavrov, A. N.; Ando, Y. *Phys. Rev. Lett.* **2003**, *90*, 227201.
(9) Khalyavin, D. D.; Barilo, S. N.; Shiryaev, S. V.; Bychkov, G. L.; Troyanchuk, I. O.; Furrer, A.; Allenspach, P.; Szymczak, H.; Szymczak, R. *Phys. Rev. B* **2003**, *67*, 214421.
(10) Soda, M.; Yasui, Y.; Ito, M.; Iikubo, S.; Sato, M.; Kakurai, K. *J. Phys. Soc. Jpn.* **2004**, *73*, 464.
(11) Maignan, A.; Caignaert, V.; Raveau, B.; Khomskii, D.; Sawatzky, G. *Phys. Rev. Lett.* **2004**, *93*, 26401.
(12) Zhou, H.; D.; Goodenough, J. B. *J. Solid State Chem.* **2004**, *177*, 3339.
(13) Taskin, A. A.; Lavrov, A. N.; Ando, Y. *Phys. Rev. B* **2005**, *71*, 134414.
(14) Zhou, Z. X.; Schlottmann, P. *Phys. Rev. B* **2005**, *71*, 174401.
(15) Baran, M.; Gatalskaya, V. I.; Szymczak, R.; Shiryaev, S. V.; Barilo, S. N.; Bychkov, G. L.; Szymczak, H. *J. Phys.: Condens. Matter* **2005**, *17*, 5613.
(16) Chernenkov, Y. P.; Plakhty, V. P.; Fedorov, V. I.; Barilo, S. N.; Shiryaev, S. V.; Bychkov, G. L. *Phys. Rev. B* **2005**, *71*, 184105.
(17) Roy, S.; Dubenko, I. S.; Khan, M.; Condon, E. M.; Craig, J.; Ali, N.; Liu, W.; Mitchell, B. S. *Phys. Rev. B* **2005**, *71*, 024419.
(18) Plakhty, V. P.; Chernenkov, Y. P.; Barilo, S. N.; Podlesnyak, A.; Pomjakushina, E.; Moskvin, E. V.; Gavrilov, S. V. *Phys. Rev. B* **2005**, *71*, 214407.
(19) Flawell, W. R.; Thomas, A. G.; Tsoutsou, D.; Mallick, A. K.; North, M.; Seddon, E. A.; Cacho, C.; Malins, A. E. R.; Patel, S.; Stockbauer, R. L.; Kurtz, R. L.; Sprunger, P. T.; Barilo, S. N.; Shiryaev, S. V.; Bychkov, G. L. *Phys. Rev. B* **2004**, *70*, 224427.
(20) Conder, K.; Pomjakushina, E.; Pomjakustin, V.; Stingaciu, M.; Streule, S.; Podlesnyak, A. *J. Phys.: Condens. Matter* **2005**, *17*, 5813.
(21) Wu, H. *Phys. Rev. B* **2001**, *64*, 092413.
(22) Wu, H. *J. Phys.: Condens Matter* **2003**, *15*, 503.
(23) Hidaka, M.; Soejima, M.; Wijesundera, R. P.; Soda, M.; Sato, M.; Choi, S.-H.; Sung, N. E.; Kim, M. G.; Lee, J. M. *Phys. Status Solidi B* **2006**, *243*, 1813.
(24) Fauth, F.; Suard, E.; Caignaert, V.; Mirebeau, I. *Phys. Rev. B* **2002**, *66*, 184421.
(25) Frontera, C.; García-Muños, J. L.; Carrillo, A. E.; Aranda, M. A. G.; Margiolaki, I.; Caneiro, A. *Phys. Rev. B* **2006**, *74*, 054406.
(26) khalyavin, D. D.; Argyriou, D. N.; Amann, U.; Yaremcmhenko, A. A.; Kharton, V. V. *Phys. Rev. B* **2007**, *75*, 134407.

10.1021/cm8021775 CCC: $40.75
Published on Web 12/04/2008

There are at least three possible reasons for these discrepancies: (i) small deviations from the ideal "O5.5" stoichiometry, (ii) variation of the degree of ordering in oxygen vacancies due to the different method of synthesis, and (iii) influence of the size of the Ln^{3+} cation.

Keeping these prospects in mind, we have tried to synthesize the lanthanum-based $LaBaCo_2O_{5.5}$ phase, which was not known up to date, and has the advantage of containing the nonmagnetic La^{3+} cation. We report herein on the synthesis, neutron diffraction, electron microscopy study, and magnetic properties of the 112 oxygen deficient ordered perovskite $LaBaCo_2O_{5.5}$. We show that the 112 matrix, characteristic of these cobaltates, contains domains with the $LnBaMn_2O_{5.5}$ structure,[31] both frameworks being closely related. Importantly, we demonstrate that $LaBaCo_2O_{5.5}$ exhibits an intermediate spin state (IS) for cobalt in the whole temperature range from 10 to 326 K.

Experimental Section

Synthesis. The synthesis of $LaBaCo_2O_{5.5}$, keeping rigorously the "O5.5" stoichiometry and a perfect layered ordering of La^{3+} and Ba^{2+} species, is delicate due to the too small size difference between La^{3+} and Ba^{2+} ions which favors their statistical distribution and to the larger size of La^{3+} compared to other lanthanides which allows large amounts of oxygen to be inserted, so that the simple $La_{0.5}Ba_{0.5}CoO_3$ perovskite is more easily obtained under normal conditions.

Thus, the successful synthesis of this phase requires several steps, using soft chemistry method, and preparing first the layered ordered double perovskite $LaBaCo_2O_6$, as previously described.[32] Stoichiometric amounts of nitrates $La(NO_3)_3 \cdot 4H_2O$, $Ba(NO_3)_2$, and $Co(NO_3)_2 \cdot 6H_2O$ were dissolved into distilled water, aided with mild heating (60 °C). After adding citric acid into the solution, the evaporation of the solvent (120 °C) resulted in amorphous dry gel which was decomposed at 600 °C for overnight to burn away the carbon and nitrogen residues. The precursor was fired at 900 °C, and then pelletized powder was sintered at 1150 °C in Ar flow (5 N) for 48 h in a plate-type platinum crucible. Heating and cooling rates were kept slow (2 °C/min) to enable better *A* cation and oxygen vacancy ordering. The intermediate low-temperature treatment was found to be crucial for the final phase formation when preparing a large sample amount. The so obtained phase has a composition close to $LaBaCo_2O_5$, and its formation occurs only in a very narrow area in the La−Ba−Co−O phase diagram as discussed by Taskin et al.[13] Note that the value of the oxygen pressure is crucial: our results suggest that the effective $p(O_2)$ has to lie between 10^{-4} and 10^{-5} atm to obtain the aimed phase, requiring high quality Ar gas for the synthesis. This as-synthesized product was then fully oxygenated at 350 °C under 130 bar O_2, leading to the tetragonal, ordered double perovskite $LaBaCo_2O_6$.

The 112 phase $LaBaCo_2O_{5.5}$ was synthesized starting from the layered double perovskite $LaBaCo_2O_6$ by employing temperature-controlled oxygen depletion. The temperature for the final thermal treatment was carefully chosen by means of various thermogravimetric (TG) measurements and then scaled up for furnace annealing. Like the other 112-type cobaltates, $LaBaCo_2O_6$ does not possess any kinetically stable plateau during oxygen removal, and therefore the control of the annealing temperature to obtain the correct oxygen content is crucial. The topotactic synthesis of $LaBaCo_2O_{5.5}$ finally took place at 590 °C in which the sample was kept for 12 h in Ar flow. The sample was then furnace cooled to room temperature.

Compared to the other $LnBaCo_2O_{5.5}$ cobaltates with smaller Ln^{3+} cations, the $LaBaCo_2O_{5+x}$ compound is extremely sensitive for oxygen intake and is oxidized in the range of 160−330 °C in one step in the presence of even a small amount of oxygen in an uncontrollable way. Nevertheless, the process is reversible. Similar behavior was observed also for $LaBaMn_2O_{5.5}$[31] and $YBaMn_2O_{5.5}$.[33,34] All of these materials require a very reductive atmosphere for their phase formation.

Characterization. The phase purity was confirmed with Philips X'pert Pro Diffractometer. Neutron powder diffraction (NPD) patterns were collected at the Institute Laue Langevin (Grenoble, France) with the high-resolution D2B powder diffractometer (λ = 1.5933 Å, T = 10−410 K). The program FULLPROF[35] was used in the Rietveld refinements of the NPD data.

For the transmission electron microscope (TEM) observations, the samples were crushed in an agate mortar in *n*-butanol, and a drop of each suspension was deposited on a carbon-coated grid. TEM studies were carried out with both JEOL 2010 and 2010F electron microscopes.

A Setaram TG 92 thermobalance was used in the thermogravitmetric (TG) annealing at the heating rate of 1 °C/min under Ar flow. Wet-chemical redox analysis by means of iodometric titrations was performed for various samples to obtain a good control of oxygen stoichiometry in each step necessary. The finely powdered specimen of 30 mg was dissolved under Ar into 1 M acetic buffer solution containing excess of KI (1 g). The released iodide, a result of the reaction between Co^{3+}/ Co^{4+} and I^- ions, was titrated with 0.015 M $Na_2S_2O_3$ solution using starch as an indicator. The $Na_2S_2O_3$ solution was standardized against 1/60 M KIO_3 solution. Each analysis was repeated 3 to 5 times to verify the reproducibility within the results, in the limit of error ± 0.01 oxygen per formula "O5.50+δ".

The magnetic properties were investigated with a SQUID magnetometer (MPMS Quantum Design) in the temperature range 10−400 K under different applied magnetic fields. The magnetic field dependent isothermal magnetization, $M(H)$, was recorded at different temperatures (after cooling down the sample from 350 K) in an applied field of 5 Tesla (T).

Results and Discussion

The wet-chemical redox analysis gave $LaBaCo_2O_{5.52\pm0.01}$ as the final stoichiometry for the studied compound. Hence, in the limit of the errors we can admit that we have reached the ideal formula. The nuclear structure was first investigated from NPD at different temperatures and then by TEM at room temperature. The magnetic structure was studied in a second step from NPD measurements, versus temperature,

(27) Barilo, S. N.; Shiryaev, S. V.; Bychkov, G. L.; Shestak, A. S.; Flavell, W. R.; Thomas, A. G.; Rafique, H. M.; Chernenkov, Y. P.; Plakhty, V. P.; Pomjakushina, E.; Conder, K.; Allenspach, P. *J. Cryst. Growth* **2008**, *310*, 1867.
(28) Frontera, C.; García-Muños, J. L.; Castaño, O.; Ritter, C.; Caneiro, A. *J. Phys.: Condens. Matter* **2008**, *20*, 104228.
(29) Jorgensen, J. E.; Keller, L. *Phys. Rev. B* **2008**, *77*, 024427.
(30) Khalyavin, D. D.; Argyriou, D. N.; Amann, U.; Yaremchenko, A. A.; Kharton, V. V. *Phys. Rev. B* **2008**, *77*, 064419.
(31) Caignaert, V.; Millange, F.; Domengès, B.; Raveau, B. *Chem. Mater.* **1999**, *11*, 930.
(32) Rautama, E.-L.; Boullay, B.; Kundu, A. K.; Caignaert, V.; Pralong, V.; Karppinen, M.; Raveau, B. *Chem. Mater.* **2008**, *20*, 2742.
(33) Karppinen, M.; Okamoto, H.; Fjellvåg, H.; Motohashi, T.; Yamauchi, H. *J. Solid State Chem.* **2004**, *177*, 2122.
(34) Perca, C.; Pinsard-Gaudart, L.; Daoud-Aladine, A.; Fernández-Díaz, M. T.; Rodríguez-Carvajal, J. *Chem. Mater.* **2005**, *17*, 1835.
(35) Rodríguez-Carvajal, J. *Physica B* **1993**, *92*, 55.

and these structural analyses were completed by magnetic measurements.

Nuclear Structure. X-ray powder diffraction (XRPD) and NPD data collected at room temperature were used in a combined refinement to obtain the neutron wavelength and accurate profile shape parameters. Additional reflections that arise from the magnetic structure (order) are yet observed at room temperature and were taken into account in the refinement. The analysis of data shows that the structure of this phase is very similar to that observed for the other $LnBaCo_2O_{5.5}$ compounds and can be described in the *Pmmm* space group with $a \sim a_P$, $b \sim 2b_P$, and $c \sim 2c_P$ cell parameters.[3,6,18,24−29] Nevertheless, several studies[18,26,29] have shown that the nuclear structure, below the paramagnetic state, could be described in the *Pmma* space group with a doubling of the *a* parameter. An attempt to refine our data with this structural model gives the same reliability factors as for the *Pmmm* model. But it is worth noting that superstructure reflections confirming the *Pmma* space group have never been observed in previous NPD studies due to the expected (calculated) weakness of these reflections. As it is not possible to prove unambiguously the correctness of the space group and that the difference between these two models is not large enough to introduce a bias in the refinement, we choose to refine all the data in the smallest unit cell, that is, in the *Pmmm* model. The combined refinement also shows that the profile of the reflections is anisotropically broadened in the XRPD data and, to a lesser extent, in the NPD data. Taking into account the anisotropic broadening in the NPD data analysis leads to a decrease of the χ^2 from 5.07 to 4.11. As the titration results indicated a slight positive deviation from the ideal oxygen "5.5" stoichiometry, the occupancy factors of the O6 (0, 1/2, 0) and the vacant site O7 (0, 0, 0), located in the La layer, were refined. The significant decrease of the χ^2 from 4.11 to 3.84 shows that there are about 8% of vacancies on the O6 site and 9% oxygen excess on the O7 site. Figure 1 shows the NPD pattern of $LaBaCo_2O_{5.5}$ at room temperature and 390 K. Crystallographic information is listed in Table 1 for measurements at 10 K, 290 K, and 390 K.

Although the refined occupancy of this excess oxygen was in good agreement with the chemical analysis, we must notice that a significant fraction of the O6 oxygen is displaced to the O7 site. A similar deviation from the perfect order between the vacant site O7 and the fully occupied site O6 was reported for a $PrBaCo_2O_{5.5}$ sample.[25] In this case, this deviation from the perfect order was interpreted as a local disorder. But it is also possible to consider that these defects are locally ordered to give in places a structure closely related to the $LaBaMn_2O_{5.5}$ structure.[31] From these results, the structure of this phase can be described as built up of a main matrix, called 112-type I cobaltate (Figure 2a), which consists of corner-shared CoO_6 octahedra and CoO_5 pyramids forming six-sided tunnels and perovskite cages where the La^{3+} and Ba^{2+} cations are sitting, respectively. The cobalt polyhedra form octahedral layers parallel to (010), interconnected through double pyramidal ribbons running along $\vec{a}$. In fact, the La^{3+} and Ba^{2+} cations alternate in the form of layers, stacked along $\vec{c}$, and this ordering is responsible for the doubling of the $\vec{c}$ parameter, similarly to what is observed in the ordered layered stoichiometric perovskite $LaBaCo_2O_6$[32,36] (Figure 2b), where $[LaO]_\infty$ and $[BaO]_\infty$ layers alternate along *c*. Then, in the 112-type I cobaltate, the doubling of the *b* parameters with respect to $LaBaCo_2O_6$, results from the 1:1 ordering of the oxygens and vacancies along that direction.

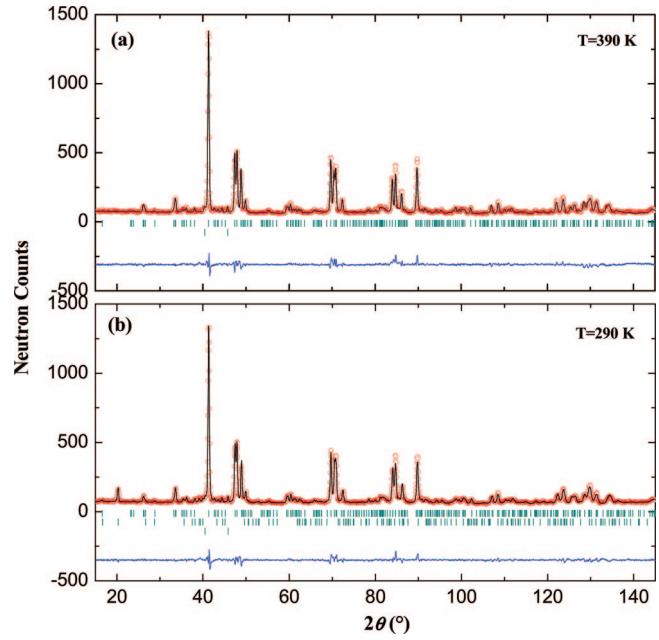

Figure 1. Rietveld refinement profiles of the neutron diffraction patterns of the $LaBaCo_2O_{5.5}$ compound at (a) 390 K and (b) 290 K. In (a), only nuclear (plus cryofurnace reflections) peaks are present, whereas in (b), magnetic reflections are already observed in the range of $2\theta = 15-40°$.

Table 1. Selected Structural Parameters of the $LaBaCo_2O_{5.5}$ Compound (Space Group *Pmmm*) Obtained from the Rietveld Refinements of the High-Resolution Neutron Powder Diffraction Data[a]

atom	site		$T = 390$ K	$T = 290$ K	$T = 10$ K
La	2o	1/2 *y* 0	$y = 0.2672(6)$	0.2679(5)	0.2670(6)
			$B = 1.00(5)$	0.67(4)	0.62(4)
Ba	2p	1/2 *y* 1/2	$y = 0.2465(8)$	0.2471(7)	0.2490(9)
			$B = 1.00(5)$	0.67(4)	0.62(4)
Co1	2q	0 0 *z*	$z = 0.244(1)$	0.249(1)	0.248(1)
Co2	2r	0 1/2 *z*	$z = 0.259(1)$	0.253(1)	0.254(1)
			$B = 0.2$	0.2	0.2
O1	4u	0 *y z*	$y = 0.2358(6)$	0.2373(6)	0.2373(6)
			$z = 0.2188(5)$	0.2199(6)	0.2193(7)
			$B = 1.51(7)$	1.33(7)	1.40(8)
O2	2s	1/2 0 *z*	$z = 0.2040(9)$	0.2023(8)	0.2039(9)
			1.8(1)	1.4(1)	1.1(1)
O3	2t	1/2 1/2 *z*	$z = 0.2433(9)$	0.2437(8)	0.2428(9)
			$B = 1.8(1)$	1.4(1)	1.3(1)
O4	1c	0 0 1/2	$B = 1.9(1)$	1.7(1)	1.3(1)
O5	1g	0 1/2 1/2	$B = 0.7(1)$	0.5(1)	0.5(1)
O6	1e	0 1/2 0	$B = 0.7(2)$	1.3(2)	1.2(2)
			$g = 0.92(3)$	0.91(3)	0.91(2)
O7	1a	0 0 0	$B = 0.9$	0.9	0.9
			$g = 0.10(2)$	0.11(2)	0.11(1)
a (Å)			3.9233(4)	3.9264(2)	3.9205(4)
b (Å)			7.9275(9)	7.9211(1)	7.8976(8)
c (Å)			7.7041(9)	7.6930(8)	7.6828(9)
R_p (%)			4.74	4.24	4.67
R_{wp} (%)			6.43	5.73	6.42
χ^2			5.22	4.66	6.32

[a] The atomic displacement parameter *B* is given in [Å^2].

(36) Nakajima, T.; Ichihara, M.; Ueda, Y. *J. Phys. Soc. Jpn.* **2005**, *74*, 1572.

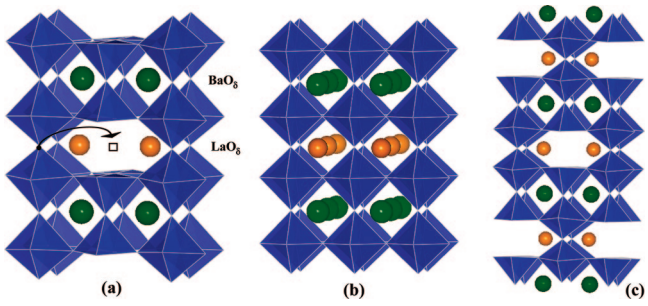

Figure 2. (a) Proposed structural model for the type I $LaBaCo_2O_{5.5}$ cobaltate prepared from (b) the layered $LaBaCo_2O_6$ double perovskite. About 9% of the main matrix consists of type II Manganite structure (c).

In other words, this main structure can be described by the stacking along $\vec{c}$ of $[CoO_2]_\infty$ layers, with $[BaO]_\infty$ and $[LaO_{0.5}\square_{0.5}]_\infty$ layers according to the sequence "$BaO-CoO_2-LaO_{0.5}\square_{0.5}-CoO_2-BaO$". (The symbol $\square$ stands for the oxygen vacancies in the $[LaO_{0.5}]_\infty$ layer.)

Now, in order to explain the deficiency and excess oxygen on O6 and O7 sites, respectively, one has to consider the structure where the O6 site is empty and the O7 site is fully occupied (Figure 2c). The latter corresponds to that of $LaBaMn_2O_{5.5}$[31] and for this reason can be called 112-type Manganite structure. Such a structure exhibits, similarly to the first one, layers of La^{3+} and Ba^{2+} cations stacked alternately along $\vec{c}$, with the same number of corner-sharing CoO_6 octahedra and CoO_5 pyramids, but differs from the latter by the fact that the pure octahedral layers have disappeared. One indeed observes quadruple ribbons of cobalt polyhedra built up of double chains of corner-shared CoO_6 octahedra, sandwiched between two single chains of CoO_5 pyramids. In summary, this 112 type II Manganite structure is simply described from the type I cobaltate structure by the shifting of one oxygen atom along $\vec{b}$ from the O6 to the O7 position in one $LaO_{0.5}$ layer out of two (see arrows in Figure 2a). It results in a quadrupling of the periodicity of the structure along $\vec{c}$.

Electron Microscopy Investigations. As shown from the Rietveld refinements of the NPD data, the structure of $LaBaCo_2O_{5.5}$ deviates from the ideal structure by a partial disorder of the oxygen atoms at the level of the $LaO_{0.5}$ layers. One indeed observes occupancy of about 90% and 10% of the O6 and O7 sites by oxygen, respectively, instead of the expected 100% and 0%. Therefore, we decided to investigate this sample by TEM in order to identify possible secondary phase, superstructures, and/or particular microstructural features.

In the Figure 3, selected area electron diffraction (SAED) confirms that the observed spots can be indexed with the *Pmmm* $a_p \times 2a_p \times 2a_p$ structure refined from powder diffraction. However, two additional features can be evidenced:

First, all the investigated crystals present twinned domains at a microscale level corresponding to the *Pmmm* $a_p \times 2a_p \times 2a_p$ structure with usually two domains (D_I and D_{II}) oriented at 90° with respect to each other (permutation of *a* and *b* axes). The zone axis patterns (ZAP) series presented in Figure 3a−c can be regarded as very representative of the examined samples. In Figure 3d, a second type of less encountered $[210]_I$ or $\langle 110\rangle_p$ ZAP is presented and where some extra weak reflections (indicated by arrows) could be indexed considering another orientation variant (D_{III}) having the *Pmmm* $a_p \times 2a_p \times 2a_p$ structure. In terms of microstructure $LaBaCo_2O_{5.5}$ appears close to the ordered $LaBaCo_2O_6$,[32] as illustrated in the bright field image (Figure 4). While the size of the twinned domains can vary significantly from one crystal to the other (Figure 4), no mottled contrast typical of the 3D domain texture of the nanoscale-ordered $LaBaCo_2O_6$ form[32] can be observed in $LaBaCo_2O_{5.5}$.

Second, in few areas of some investigated crystals, very weak extra reflections that cannot be indexed considering the *Pmmm* $a_p \times 2a_p \times 2a_p$ structure are actually observed as illustrated for the $[410]_I$ ZAP in Figure 3e. This indicates that, besides twinning, these crystals possess locally a structure different from the 112-type cobaltate. The information available by SAED about such superstructures is blurred due to the superposition with the reflections coming from the *Pmmm* $a_p \times 2a_p \times 2a_p$ domains. Nonetheless, from the positions of these extra spots, common characteristics can be summed up and imply, notably, the doubling of one of the $2a_p$ parameter together with a centering of the cell. Considering the literature on the 112-type compounds, a part of these extra spots can be indexed considering the *Cmmm* $2a_p \times 4a_p \times a_p$ cell corresponding to the $LaBaMn_2O_{5.5}$ compound.[31] This is in agreement with the results of the NPD refinements where the occupancies obtained for the O6 and O7 atomic positions can be locally attributed to a different vacancy/oxygen ordering leading notably to the existence of faulted zones having a centered structural motif (112 type II). This tendency is evidenced by SAED but also visible in HREM for instance looking at one of the $\langle 110\rangle_p$ directions (Figure 5). The *Pmmm* $a_p \times 2a_p \times 2a_p$ structure is established all over the viewing area but locally in the area encircled the structural motif is clearly different and presents a centering also evidenced in the Fourier transform.

Is it important to note here that due to the systematic presence of 112 type I oriented domains (eventually combined with 112 type II domains), we cannot conclude about the existence of the doubling of the a parameter (with a *Pmma* space group) as proposed in previous works for lanthanides such as Gd, Tb, Dy, and Ho.[16,18,27,29] Lastly, it is worth mentioning that no $3a_p \times 3a_p \times 2a_p$ superstructure observed by TEM for lanthanides such as Ho[3] and for $YBaCo_2O_{5+\delta}$ compound with $\delta = 0.44$[37] can be evidenced in this $LaBaCo_2O_{5.5}$ sample. This is in agreement with a δ slightly superior to 0.5 and would indicate that oxygen vacancies are evenly distributed since such a superstructure is very easily formed as soon as $\delta < 0.5$ [see ref 38 as an illustration].

Magnetic Properties. The magnetization and susceptibility curves versus temperature, $M(T)$, measured in the range 10−400 K, under external fields between 0.01 and 5 T (Figure 6) are similar to those previously observed for other lanthanides,[1−18] that is, in the whole temperature range the

(37) Akahoshi, D.; Ueda, Y. *J. Solid State Chem.* **2001**, *156*, 355.
(38) Pautrat, A.; Boullay, P.; Hébert, S.; Caignaert, V. *Phys. Rev. B* **2007**, *76*, 214416.

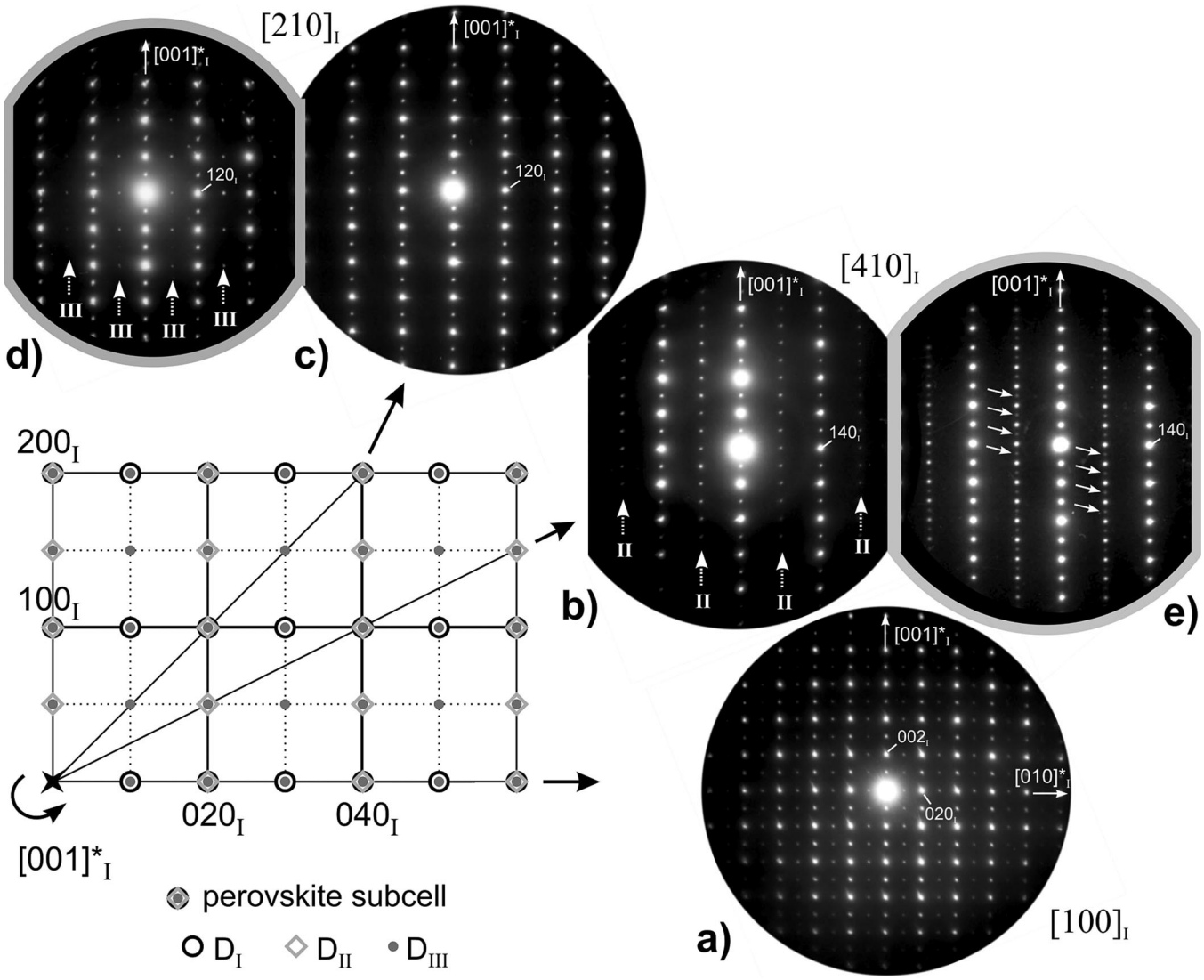

Figure 3. Typical SAED patterns observed for $LaBaCo_2O_{5.5}$. The [100] zone axis patterns (ZAP) displayed in (a) are the most characteristic. The doubling of both cell parameters along the *b* and *c* directions with respect to the perovskite subcell can be observed. By performing tilting experiments, one evidences the systematic presence of 90° oriented domains with either two diffracting domains (D_I and D_{II}) as illustrated in the ZAP series (a−c) or less frequently three diffracting domains (D_I, D_{II}, and D_{III}). In this last case, the third 90° oriented domains (D_{III}) can be revealed on ZAP such as $[210]_I$ presented in (d). A schematic representation of the reciprocal space with the contribution of each diffracting domains is given in order to facilitate the reading of the ZAP (a−d). For some of the investigated crystals, supplementary weak spots can be observed on ZAP such as $[410]_I$ (see arrows in e). These reflections cannot be indexed considering a *Pmmm* $a_p \times 2a_p \times 2a_p$ diffracting domain.

system exhibits several magnetic transitions from paramagnetic (PM) to ferromagnetic like (FM) to antiferromagnetic (AFM) as T decreases from 400 K to 10 K. The sudden increase of the magnetic susceptibility at $T_C = 326$ K indicates a PM/FM transition. Nevertheless, the highest value of the magnetic moment (M_{FC}^{ST}) close to room temperature is only of 0.23 μ_B/f.u. and there is no saturation in the ZFC and FC magnetization data. The sharp decrease in the magnetization indicates a FM/AFM transition at $T_N = 260$ K. The magnetization remains almost constant in the low temperature AFM state for both the ZFC and the FC data, with a significant thermomagnetic irreversibility in that region. Moreover, the magnetic irreversibility between ZFC and FC remains well discernible even at higher field ($H \geq 5$ T). It can be seen from Figure 6b that a high field basically affects the FM−AFM competition, which in turn suppresses the magnetization drop below the T_N. Thus, with increasing the external magnetic field, the FM state (in the temperature region $260 \leq T \leq 326$) becomes more stable, but T_N shifts to lower temperature. As a result, the FM region expands in the temperature scale (see Figure 6b). In the AFM phase, the nonzero value of magnetization down to low temperature signifies the presence of some kind of FM-like interactions, as shown for instance at $T \sim 90$ K, where some weak magnetic transition (indicated by an arrow in Figure 6b) is evidenced.

The inset of Figure 6a shows the inverse magnetic susceptibility versus temperature plot in the temperature range of 220−400 K. This follows a simple Curie−Weiss behavior in the 335 K $\leq T \leq$ 400 K range giving a PM Weiss temperature (θ_p) of ∼−290 K and an effective PM magnetic moment (μ_{eff}) of 3.72 μ_B/Co. The large negative θ_p value for ordered $LaBaCo_2O_{5.5}$ sample indicates the existence of AFM type interactions in the high temperature region. The obtained μ_{eff} value from the paramagnetic region

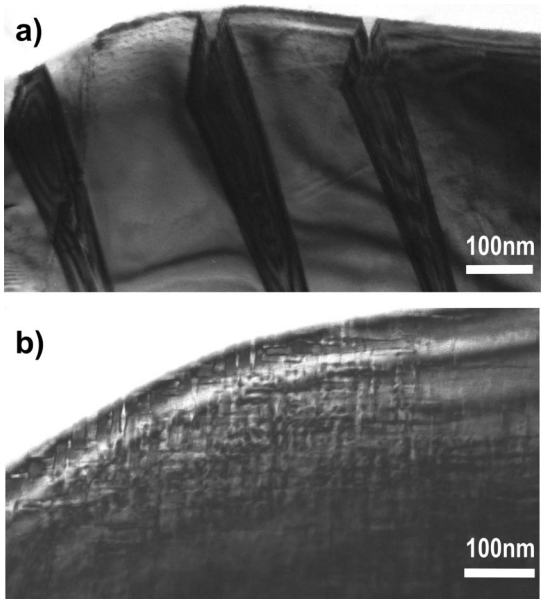

Figure 4. As expected from SAED experiments, the bright-field images obtained for $LaBaCo_2O_{5.5}$ reveal the existence of twinned domains whose size can vary from one crystal (a) to the other (b) and can be as small as 10 nm.

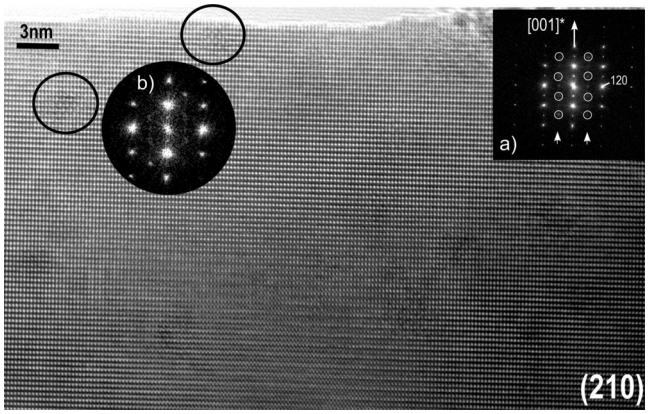

Figure 5. (210) HREM image and the corresponding Fourier transform (right upper corner in a) (a) in the rows indicated by arrows, some of the spots (encircled) are not compatible with a *Pmmm* $a_p \times 2a_p \times 2a_p$ cell even considering oriented domains. More precisely, one can notice areas where the contrast is different from the rest of the image and where bright spots exhibit a centered motif (see zones indicated by a large black circle). In (b), the Fourier transform performed on such areas corroborates the information obtained by SAED. Besides the 112-type $LaBaCo_2O_{5.5}$ matrix, domains compatible with a 112 $LaBaMn_2O_{5.5}$-type structure are evidenced (see text).

corresponds to a situation where the Co^{3+} ions are mainly in the intermediate spin (IS) state. This last point is also supported by the study of the magnetic structure by NPD, which will be detailed further. The sharp drop in inverse susceptibility near T_C, similar to that observed for $YBaCo_2O_{5.5}$ and $GdBaCo_2O_{5.5}$,[8,37] cannot be interpreted as a ferromagnetic ordering of the IS-Co^{3+} ions in $LaBaCo_2O_{5.5}$, due to the too small value of their magnetic moment (0.23 μ_B/f.u.).

To further confirm the FM-like interactions below T_C = 326 K, we have studied the magnetic field dependent isotherm magnetization, $M(H)$, at six different temperatures as shown in Figure 7. The $M(H)$ curve at 300 K shows a prominent hysteresis loop with a remanent magnetization,

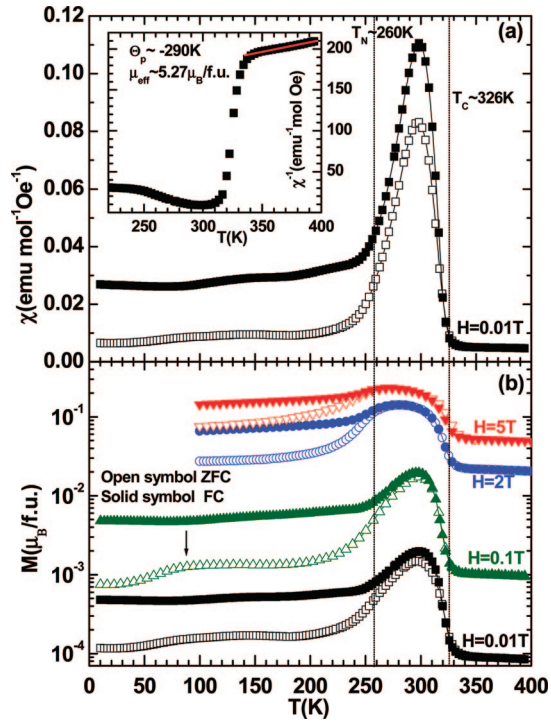

Figure 6. Temperature dependent ZFC (open symbol) and FC (solid symbol) magnetization behavior of ordered $LaBaCo_2O_{5.5}$; (a) magnetic susceptibility, χ, under $H = 0.01$ T (inset figure shows the inverse magnetic susceptibility, χ^{-1}, versus temperature plot and solid line is Curie−Weiss fitting) and (b) magnetic moment, M(T), measured in different magnetic fields ($H = 0.01$, 0.1, 2, and 5 T).

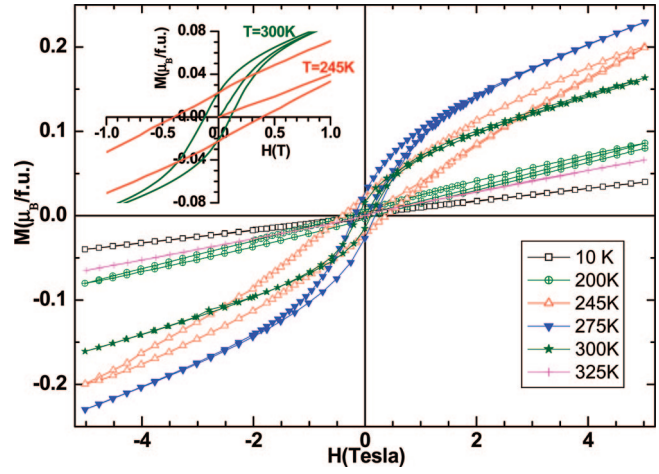

Figure 7. Magnetic field dependent isotherm magnetization, $M(H)$, of ordered $LaBaCo_2O_{5.5}$ at six different temperatures. The inset figure shows the expanded version for lower magnetic fields at 245 and 300 K.

M_r, and a coercive field, H_C, values of 0.02 μ_B/f.u. and 0.1 T, respectively, indicating a FM-like state below T_C. Nevertheless, the maximum value of the magnetic moment measured in 5 T (0.23 μ_B/f.u.) at 275 K is much smaller than the theoretical spin-only value (4 μ_B/f.u.) of Co^{3+} in the IS state. Therefore, the FM like behavior of this compound is due to a canting of the magnetic spin alignment or to a ferrimagnetic behavior. Although there are some controversies in the literature to explain these FM-like features, this behavior is prominent for the present system and subject to further investigations. It is worth pointing out that at low temperature in the AFM state, some FM-like phase is still present as evidenced from the $M(H)$ behavior,

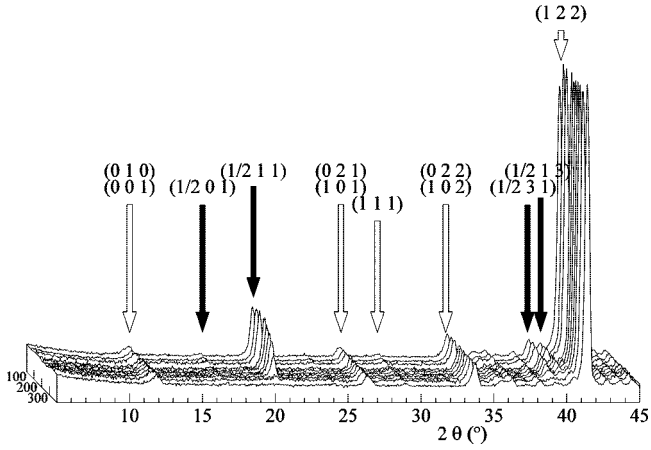

Figure 8. Thermal evolution of the neutron powder diffraction patterns registered with D2B in the range of 10−390 K. The reflections *hkl* are indexed with white ($h = n$) and black ($h = n + 1/2$) arrows applying the *Pmmm* ($\mathbf{k}$ = 1/2, 0, 0) unit cell.

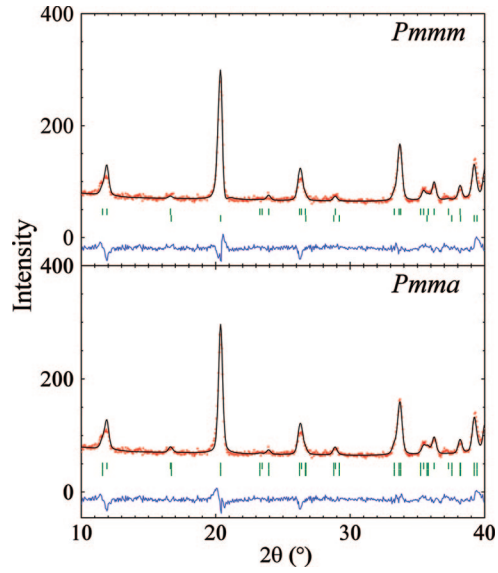

Figure 9. Magnification on the magnetic reflections appearing at 2θ = 10−40° and their Rietveld refinements with *Pmmm* ($\mathbf{k}$ = 1/2, 0, 0; top) and *Pmma* ($\mathbf{k}$ = 0, 0, 0; bottom) models at 10 K.

with a finite value of the coercive field. Interestingly, the highest coercive field value of 0.4 T (at 245 K) is obtained in the AFM region compared to the value of 0.1 T in the FM region (at 300 K). For comparison the H_C values in the FM and AFM regions we have replotted the $M(H)$ data for lower fields in the inset of Figure 7. The H_C values in the AFM region (275−200 K) are larger than in the FM region, and finally at 10 K, the $M(H)$ behavior becomes linear akin to AFM state.

Magnetic Structure. The NPD patterns of $LaBaCo_2O_{5.5}$, registered for different temperatures (Figure 8), show additional reflections, originating from magnetic interactions in the temperature range from 10 to 330 K. These reflections are compatible with a G-type magnetic structure either with propagation vector $\mathbf{k}$ = (1/2, 0, 0) with respect to the $a_p \times 2a_p \times 2a_p$ nuclear cell (*Pmmm*) as proposed for $NdBaCo_2O_{5.5}$[24] or with a propagation vector $\mathbf{k}$ = (0, 0, 0) with respect to the $2a_p \times 2a_p \times 2a_p$ nuclear cell (*Pmma*) as shown for $LnBaCo_2O_{5.5}$ compounds with Ln = Tb, Y, Dy.[18,26,27] As previously observed for the other "112" cobaltates, the intensity of these reflections decreases as T increases, the reflections becoming very weak but remaining still sharp at T = 330 K. This feature is consistent with the magnetization data, showing a transition from an ordered magnetic state to the paramagnetic state at T_C = 326 K (Figure 6).

In fact, $LaBaCo_2O_{5.5}$ differs from the other 112 cobaltates by the fact that no transition of its magnetic structure is detected below T_N = 260 K although its magnetization vanishes below this temperature (Figure 6), like for the other "112" oxides. This suggests that the antiferromagnetic phase that appears below T_N = 260 K is also G-type but, in contrast to the other lanthanides, does not exhibit a propagation vector $\mathbf{k}$ = (0, 0, 1/2) with respect to the $2a_p \times 2a_p \times 2a_p$ (*Pmma*) structure,[18,26,29] but keeps the $\mathbf{k}$ = (0, 0, 0) vector. Such a difference can be explained by the size of La^{3+} which is significantly larger than other lanthanides and consequently influences significantly the crystal field.

Concerning the nature of the magnetic phase, formed in the window of 260−326 K, the low value of the magnetization, of about 0.12 μ_B/Co, like for the other lanthanides (Tb, Y, Dy),[18,26,29] does not allow an accurate study of its magnetic structure. Bearing in mind that the description of the magnetic structure in the nuclear cell $a_p \times 2a_p \times 2a_p$ (*Pmmm*) with a propagation vector $\mathbf{k}$ = (1/2, 0, 0) cannot explain the spontaneous magnetization observed, it is most likely that the magnetic phase is ferrimagnetic with a nuclear cell $2a_p \times 2a_p \times 2a_p$ (*Pmma*) and a propagation vector $\mathbf{k}$= (0, 0, 0) as described by Plakhty et al.[18] and Khalyavin et al.[26] Nevertheless, the latter requires the existence of at least four magnetic sites[26] so that the *Pmma*, $2a_p \times 2a_p \times 2a_p$, magnetic structure is the only one possible if one admits the absence of phase separation. This model also involves the existence of magnetic reflections h, k, l with $h = 2n$ and $h = 2n + 1$. Unfortunately, the magnetic reflections with $h = 2n$ are too weak or too close to the nuclear reflections to be observed or even detected as previously shown.[26] As a consequence, refinements in the *Pmma* space group cannot give reliable results with our data, when the number of refined parameters is higher than two. In contrast, the *Pmmm* model, though it does not explain the spontaneous magnetization, can give an approximate idea of the magnetic structure since it involves only two magnetic sites and allows a stable refinement of the data. The calculations at 10 K lead to magnetic moments of 2.4 μ_B and 1.7 μ_B for octahedral and pyramidal coordination, respectively. Despite the crudeness of the model, these results show that the structure is fairly well ordered and that the Co^{3+} ions remain in the intermediate spin state (S = 1) in the whole temperature range. Refinements in the *Pmma* space group would require constraints on the magnetic moments. Nevertheless, we have tested refinements in the *Pmma* model with different constraints in the ferrimagnetic region and at 10 K. By constraining the moments to be equal at the pyramidal site, we find the residual moment in the ferrimagnetic state to be of 0.2 μ_B in the octahedral site which is consistent with the previous results[18,26] and our magnetization data. With the same constraints at 10 K, we obtain moments practically of the same value as with the *Pmmm* model. For comparison,

Figure 9 shows the magnification of the obtained Rietveld profiles for both *Pmmm* and *Pmma* models at 10 K, refined as described above.

Conclusions

In this study, we have shown the possibility to synthesize the ordered $LaBaCo_2O_{5.5}$ cobaltate in spite of the small difference between La^{3+} and Ba^{2+} by controlling the synthesis carefully by a several steps method. From a combined NPD and EM study, we have observed that the layered structure of this phase consists of a main matrix known for the lanthanides, called type-I cobaltate (at about 92%), containing type-II Manganite domains (at about 8%) isotypic to $LaBaMn_2O_{5.5}$, both structures being built up of CoO_5 pyramids and CoO_6 octahedra and differing only by the shifting of one oxygen atom along *b* per $La_2Ba_2Co_4O_{11}$ formula.

The magnetic properties of this phase and the study of its magnetic structure show that it exhibits antiferromagnetic to ferrimagnetic to paramagnetic transitions, similar to the other lanthanide cobaltates with $T_N = 260$ K and $T_C = 326$ K. Nevertheless, $LaBaCo_2O_{5.5}$ differs from the other 112 cobaltates by its G-type antiferromagnetic structure below 260 K, which keeps the same symmetry as its ferrimagnetic phase (260−326 K). Such a difference is explained by the larger size of lanthanum compared to other lanthanides and may modify the crystal field and induce some local disorder on the cationic sites.

Finally the refinements of the magnetic structure in the *Pmmm* space group, though they lead only to an approximate model, are of capital importance since they show that the latter is well ordered and especially that Co^{3+} remains in the intermediate spin state in the whole temperature range.

The study of the electric transport properties of this phase are in progress in order to understand the relationships between the magnetic transition and the resistive transition which both appear at the same temperature ($T_C = 326$ K).

Acknowledgment. E.-L.R. thanks the Finnish Cultural Foundation for their financial support.

CM8021775